Numerical Analysis of Injection Molding of Glass Fiber Reinforced Thermoplastics. Part 1: Injection Pressures and Flow

JOSEPH P. GREENE

Manufacturing Center, A/MD-33
General Motors Corporation
Warren, Michigan 48090-9010

and

JAMES O. WILKES

Department of Chemical Engineering
The University of Michigan
Ann Arbor, Michigan 48109-2136

Numerical calculations of flow and injection pressures during injection molding of fiber-filled thermoplastics are compared to experimental measurements. The flow is modeled as a 2-D, nonisothermal, free-surface flow with a new viscosity model dependent upon temperature, pressure, and fiber concentration. The steady-state viscosity model is developed to account for the fiber-concentration and shear-thinning viscosities of the polymer based upon combining the Dinh-Armstrong fiber model with the Carreau viscosity model. The new model has four parameters, three from the Carreau model and one from Dinh-Armstrong for fiber concentrations. The new model calculates reasonably well the steady-state viscosity of fiber-filled polypropylene over the shear rate range of 0.01 s^{-1} to 20 s^{-1}. The numerical work successfully describes the flow of fiber-filled polymers during injection molding using finite-difference solutions for the transport equations and marker particles to track the flow front. The comparisons between the calculated and measured pressure drops for an injection molded part were reasonable for the unfilled and fiber-filled polypropylene materials. The pressure drop comparison is very good for slow fill of a base case resin, Himont polypropylene, but not as good for fast fill of the resin. The pressure drop comparison is very good for fast fill of glass-filled resin, DSM polypropylene with 10% and 20% short fibers, but not as good for slow fill of the resin and resin plus fibers.

INTRODUCTION

Numerical simulation of injection molding has been of considerable research interest over the past twenty years. Initially, researchers modeled the flow during injection molding as a Newtonian material in a fully developed one-dimensional flow. Mavridis *et al.* (1) considered Newtonian and shear-thinning fluids advancing with a flow front inside two-dimensional channels and tubes. Williams and Lord (2) and Huang *et al.* (3) expanded the flow analysis to two dimensions with thermal and pressure effects during the filling of the gate and fountain regions. Harry and Parrott (4) and Berger and Gogos (5) developed appropriate constitutive equations to describe thermal and pressure influences upon the viscosity. Several authors (6–8) studied the flow of polymers in thin cavities of arbitrary planar geometry. In particular, Hieber and Shen (7) demonstrated a finite element–finite difference method formulation with a two-step, predictor-corrector procedure for tracking the advancing melt front. Chiang *et al.* (9) proposed a unified theoretical model to simulate the filling and post filling aspects of injection molding. Two excellent texts describing the theory and numerical aspects of injection molding simulation are given by Tucker (10) and Isayev (11). Finite element techniques, especially with the Galerkin formulation, have been used by several researchers (12–14) to study the viscoelasticity of polymers and is better explained elsewhere (15). Viscoelasticity is very impor-

tant in the processing of polymers and can be represented with integral constitutive equations (16–18). The FEM solution approach with integral constitutive equations generally requires a super computer to solve the continuity, flow, and energy equations. For speed and efficiency in representing the polymer flow in industrial applications finite difference techniques are used with the well-known Marker-and-Cell (MAC) procedure.

Several commercial finite element-finite difference codes are available that simulate the mold filling of polymers during injection molding, e.g., FLOW-3D™ (19), Moldflow™ (20), and C-Flow™ (21). The last two packages also simulate the packing and cooling phases of injection molding and are generally considered state-of-the-art CAE tools. Moldflow™ and C-Flow™ describe the advancement of the flow front using a layered 2-D flow approach and a FEM grid representing the interested geometry.

Very few researchers have incorporated fiber-filled polymer melts into the flow analysis, because of the absence of an appropriate constitutive equation. Ghosh *et al.* (22) examined the applicability of the conformation tensor to describe fiber orientation. Advani and Tucker (23) developed a second-ordered rank tensor to describe the fiber orientation of fiber-filled polymers. Additional researchers (24–26) extended the work of Advani and Tucker in several test cases to predict fiber orientation. Typically, the viscosity of fiber-filled polymers is measured experimentally and then read into the flow analysis program. Alternatively, this research models the viscous response of the fiber-filled system by combining the Dinh-Armstrong fiber model (27) with the Carreau viscosity model. The new model, a modified Carreau model is added to a commercial free-surface flow analysis package, FLOW-3D. The results calculate the flow, cavity pressures, and temperatures of the fiber-filled thermoplastics by incorporating the energy equation into the flow program, by incorporating the shear rate, temperature, and pressure effects on the viscosity, and lastly, by incorporating fiber-orientation effects on the viscosity and the flow field. This work is a portion of a research work by Greene (28) in the study of fiber orientation during the flow of fiber-filled thermoplastics. This work is preceded by an investigation by Greene and Wilkes (29) into the effects the fibers have on the steady-state and dynamic viscous properties of three thermoplastic materials, and is followed by a numerical analysis study by Greene and Wilkes (30) that predicts fiber orientation during injection molding.

Fluid Equations of Motion

During the filling stage of injection molding, the polymer passes through three flow regions: the gate, the fully developed, and the fountain regions, as shown in *Fig. 1*. In a typical end-gated, thin-walled cavity, the gate region is characterized by radial flow, the fully developed region by a dominant parallel-velocity component, and the fountain region by a free-surface flow. The objective of the flow analysis is to obtain pressure and velocity distributions for a thermoplastic material in a closed cavity by solving the momentum and energy transport equations with an appropriate constitutive equation. The flow of the polymer in a closed die is modeled as a nonisothermal flow of a non-Newtonian material between two walls. The thin-walled flow is governed by the equation of continuity, momentum, and energy transport. The equations are as follows:

$$\text{Continuity } \nabla \cdot u = 0$$

$$\text{Momentum } \frac{Du}{Dt} = -\nabla p + \nabla \cdot \tau + \rho g$$

$$\text{Energy } \rho \hat{C}_p \frac{DT}{Dt} = \nabla \cdot k \nabla T + \frac{1}{2} \eta(\dot{\gamma} \cdot \dot{\gamma})$$

Here, u is the velocity vector, τ is the shear stress tensor, ρ is the pressure, g is the gravity term, D/Dt denotes the material derivative, T is the temperature vector, and ρ, η, $\hat{C}_p$, k are the fluid density, viscosity, heat capacity, and thermal conductivity.

The flow of a polymer material in a thin-walled cavity in a planar geometry can be written in terms of two dimensions (with z being the thickness direction). The continuity equation for constant density is

$$\frac{\partial(u)}{\partial x} + \frac{\partial(v)}{\partial y} = 0 \tag{1}$$

Here, u represents the velocity in the x-direction and v represents the velocity in the y-direction. The equations of motion and energy for a Generalized Newtonian fluid are

$$\frac{\partial u}{\partial t} + \left\{ u \frac{\partial u}{\partial x} + v \frac{\partial u}{\partial y} \right\} = -\frac{\partial p}{\partial x} + \frac{\partial}{\partial z} \left(\eta \frac{\partial u}{\partial z} \right) + g_x \tag{2}$$

$$\frac{\partial v}{\partial t} + \left\{ u \frac{\partial v}{\partial x} + v \frac{\partial v}{\partial y} \right\} = -\frac{\partial p}{\partial y} + \frac{\partial}{\partial z} \left(\eta \frac{\partial v}{\partial z} \right) + g_y \tag{3}$$

$$\rho \hat{C}_p \left\{ \frac{\partial T}{\partial t} + u \frac{\partial T}{\partial x} + v \frac{\partial T}{\partial y} \right\} = \frac{\partial}{\partial z} \left(k \frac{\partial T}{\partial z} \right) + \eta \dot{\gamma}^2 \tag{4}$$

In these equations, g_x and g_y are body accelerations, and the other terms are defined as before. In the above expressions, the wall shear stresses in the three directions are modeled by assuming a zero tangential velocity on the portion of any area closed. Mesh boundaries are an exception because they can be assigned non-zero tangential velocities.

The boundary conditions are no-slip at the wall, axisymmetric at the centerline, and free surface at the flow front. The initial conditions are for a constant wall temperature and a constant mass source at the entrance. The boundary conditions in the gapwise direction are

$$u = v = w = 0; \qquad T = Tw \quad \text{at } z = b$$

and

$$\frac{\partial u}{\partial z} - \frac{\partial v}{\partial z} = \frac{\partial T}{\partial z} = 0; \qquad w = 0 \quad \text{at } z = b$$

where b denotes the half thickness and $T = Tw$ the wall temperature. At the free surface, the tangential stress condition is zero normal velocity, $n \cdot u = 0$, and zero tangential stress.

The energy equation denotes energy exchange in the thickness direction between the fluid and the wall. The primary limitation of the structural-heat-transfer model is the simplicity of the heat-transfer coefficient correlation. During this analysis the heat transfer coefficients are implemented as independent functions.

Numerical Approximations

FLOW-3D is a descendant of the well-known marker-and-cell (MAC) finite-difference technique and the implicit-continuous fluid-Eulerian (ICE) technique, [31]. The MAC method is one of the first techniques to use pressure and velocity as the primary dependent variables in solving problems involving complicated free-surface motions. MAC employs distribution of marker particles to define fluid regions, and simply set free-surface pressures at the centers of cells defined to contain the surface. In 1981, a proprietary three-dimensional extension of the MAC method was established by Flow Science, Inc., as the basis of the present FLOW-3D code. For polymers, the code was updated with an implicit viscous-stress solution technique and with a subroutine that introduces a shear-rate dependency on the viscosity, so as to model non-Newtonian viscous flows.

FINITE-DIFFERENCE APPROXIMATIONS

FLOW-3D numerically solves the equations of motion and energy using finite-difference approximations in three dimensions. Though FLOW-3D is capable of modeling compressible flows, the scope of this chapter will encompass only incompressible flows. For incompressible fluids, the density is constant and the full density transport equation reduces to the incompressibility condition.

FLOW-3D numerically solves the equations of motion and energy using finite-difference approximations. The flow region is divided into a mesh of fixed rectangular cells. With each cell there are associated local average values of all dependent variables. All variables are located at the center of the cell except for velocities, which are located at the center of the cell faces. Curved obstacles, wall boundaries, or other geometric features are embedded in the mesh by defining the fractional face areas and fractional volumes of cells that are open to flow.

For calculations performed with the energy option, FLOW-3D allows the transfer of heat between fluid and structural material called a heat structure. Heat structures may be either internal obstacles or walls at the computational mesh boundaries. FLOW-3D calculates heat transfer from boundaries having a known temperature, a specified heat flux, or a specified internal power source. The primary limitation of the structural-heat-transfer model is the simplicity of the heat-transfer coefficient correlation. All heat-transfer coefficients are implemented as independent functions.

As in the MAC method, a control-volume approach is used to approximate the governing equations numerically. For each control volume, surface fluxes, surface stresses, and body forces are computed in terms of surrounding variable values. The momentum and continuity equations are used to compute velocity at the face of the cells and pressures at the centers. Most terms in the equations are evaluated using current time-level values (explicit formulation) of the local variables. Pressures and velocities, though, are coupled implicitly by using time-advanced velocities in the continuity equation. The semi-implicit formulation results in coupled sets of equations that are solved iteratively using two methods, a successive over-relaxation (SOR) method and a special alternating-direction, line-implicit method (SADI).

A generic form for the finite-difference approximation of the momentum equation in MAC-type methods is:

$$u^{n+1}_{i,j,k} = u^{n}_{i,j,k} + \Delta t^{n+1}\left[-\frac{(p^{n+1}_{i+1,j,k} - p^{n+1}_{i,j,k})}{\rho \Delta x^{n}_{i+1/2,j,k}} + G_x - FUX - FUY - FUZ + VISX - B_x - \tau_{wall,x}\right] \tag{5}$$

$$v^{n+1}_{i,j,k} = v^{n}_{i,j,k} + \Delta t^{n+1}\left[-\frac{(p^{n+1}_{i,j+1,k} - p^{n+1}_{i,j,k}) R_{i,j+1/2,k}}{\rho \Delta y^{n}_{j+1/2,k}} + G_y - FVX - FVY - FVZ - VISY - B_y - \tau_{wall,y}\right] \tag{6}$$

$$w^{n+1}_{i,j,k} = w^{n}_{i,j,k} + \Delta t^{n+1}\left[-\frac{(p^{n+1}_{i,j,k+1} - p^{n+1}_{i,j,k})}{\rho \Delta z^{n}_{i,j,k+1/2}} + G_z - FWX - FWY - FWZ - VISZ - B_z - \tau_{wall,z}\right] \tag{7}$$

Here, the code convention is that all fractional indices are decreased to the nearest whole integer. For example, the velocity at $(i + \frac{1}{2})$, which is located at on the cell face between cells (i, j, k) and $(i + 1, u, k)$ is denoted by $u^{n}_{i,j,k}$. The term $(\rho\Delta x)_{i+1/2,j,k}$ refers to the average of $(\rho\Delta x)_{i,j,k}$ and $(\rho\Delta x)_{i+1,j,k}$. R again refers to Cartesian or cylindrical geometries. A superscript n refers to the n^{th} time step. The advection and viscous acceleration terms have obvious meaning; e.g., FUX refers to the advective flux of u in the x-direction, $VISX$ is the x-component viscous acceleration term; B_x is the flow loss for a baffle normal to the x-direction; τ_w is the viscous wall acceler-

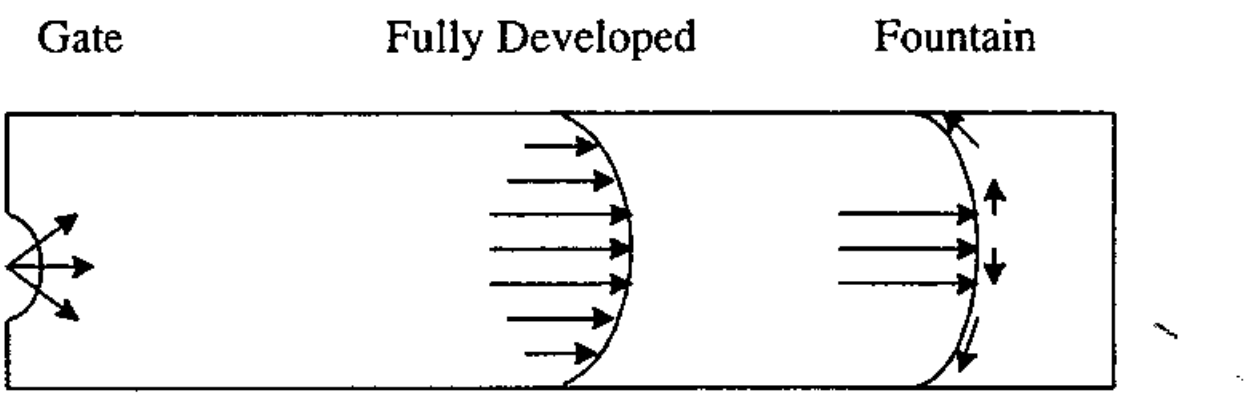

Fig. 1. Flow regions during injection molding.

ation in the x-direction; and G_x includes gravitational, rotational, and general noninertial accelerations. These terms are all evaluated using old time level values, n, for velocities.

In FLOW-3D a modified donor-cell approximation was developed by Hirt and Sicilian (32) that retains its accuracy in a variable mesh and reduces to a conservation difference expression when the fluxes in the nonconservative form $u \cdot \nabla u$. In the new approximation, the donor-cell method is combined with the centered-difference approximation into a single expression with a parameter α that controls the relative amount of each. The general form of this approximation for the advective flux term $FUX = (A_x/V)\, u\Delta u/\Delta x$ is

$$FUX = \frac{(1/2)(\Delta x_i + \Delta x_{i-1})}{(\Delta x_i VF_{i,j,k} + \Delta x_{i-1} VF_{i-1,j,k})} \cdot \left\{ \begin{array}{l} \left[\frac{(1-\alpha)}{2}((AFR)_{i-1,j,k} u_{i-1,j,k} + (AFR)_{i,j,k} u_{i,j,k})\right] \frac{(u_{i+1,j,k} - u_{i,j,k})}{\Delta x_{i-1}} \\ \frac{(1+\alpha)}{2}[(AFR)_{i,j,k} u_{i,j,k} + (AFR)_{i-1,j,k} u_{i-1,j,k})] \frac{(u_{i,j,k} - u_{i-1,j,k})}{\Delta x_i} \end{array} \right\} \quad (8)$$

Here, AVF, and R are coefficients for each cell and were previously defined as the area fraction, VOF function, and geometry coefficient.

If the mesh is uniform, *Eq 8* reduces to a spatially second-order accurate, centered-difference approximation when $\alpha = 0$. When $\alpha = 1$, the first-order, donor-cell approximation is recovered. In either case, the method reduces to the correct zeroth order expression in a variable mesh. The underlying idea from *Eq 8* is to weight the upstream quantity being fluxed more than the downstream value. The weighting factors are $(1 - \alpha)$ and $(1 - \alpha)$ for the upstream and downstream directions, respectively. This type first-order approximation scheme is used for all advective flux terms appearing in the momentum equations, *Eqs 5, 6,* and *7*. All other acceleration terms in the momentum equations are approximated by standard centered differences.

In some cases, however, it may be too costly to use the mesh resolution necessary for an accurate first-order solution. When this happens it may be useful to use a second-order accurate approximation for the advective and viscous accelerations. The essence of this optional scheme is a double pass through the advective and viscous subroutines.

MODIFICATIONS TO FLOW-3D FOR INJECTION MOLDING MODELING

The non-Newtonian rheological behavior of polymer melts is of great importance during injection molding. Shear rate and temperature dependence of the polymer viscosity must be incorporated into any simulation program. Recently, a subroutine was added to FLOW-3D to include a shear-rate dependency to the viscosity according to the Carreau relationship, which is an essential requirement for modeling shear-thinning, thermoplastic materials. Additionally, the viscosity subroutine was modified in this research to include temperature and pressure effects. The viscosity is a strong function of temperature and pressure. These are detailed below.

Temperature-Dependent Viscosity

Newton's law of viscosity describes the rheological behavior of an important class of fluids, called Newtonian fluids, that have a constant viscosity that depends upon only the temperature and pressure and not the level of applied stress or the resulting velocity gradient. The temperature dependency can be approximated by (33):

$$\mu(T) = \mu(T_0) e^{[\Delta E \cdot RT_0 (T - T_0)/T]} \quad (9)$$

Here, μ is the Newtonian viscosity, ΔE is the activation energy for flow, and R is the gas constant. The viscosity equation can be applied to a shear-dependent viscosity in the following relationship:

$$\eta(\dot{\gamma}, T) = \eta_{T_0}(\dot{\gamma}) e^{[\beta(T - T_0)/T]} \quad (10)$$

Here, η is the shear-rate-dependent viscosity and B is an empirical constant, which is found from rheometric data.

Pressure-Dependent Viscosity

Because of the high pressures encountered in high-speed injection molding, the slight compressibility of polymers cannot be ignored. The P-V-T relationship is very complicated and is beyond the scope of this work and is described elsewhere (33, 10). The pressure dependency on the viscosity can be represented in a similar fashion as the temperature, as

$$\eta(\dot{\gamma}, P) = \eta_0(\dot{\gamma})e^{\beta P} \quad (11)$$

where β is an empirical constant from viscosity-shear rate data at various pressures.

Fiber-Concentration-Dependent Viscosity

The third modification to the computer program is the inclusion of a fiber concentration function on the viscosity. The Carreau model is modified with the Dinh-Armstrong theory. The Carreau model is

$$\frac{\eta}{\eta_0} = [1 + (\lambda\dot{\gamma})^2]^{(n-1)/2} \quad (12)$$

The effects of fibers on the viscosity can be modeled as a product of the fiber concentration function, $f(\phi)$, and the viscosity of the neat resin η_s, described by the Carreau model. The Carreau model is a three-parameter model with empirical constants n (power law index), η_0 (zero-shear-rate viscosity), and λ (time constant). Since the three parameters describe the shear-thinning aspects of the polymer and the fibers effects these aspects, then the individual parameters can be modeled as functions of the fiber concentration function, $f(\phi)$, introduced by Bibbo *et al.* (34) and given by

$$f(\phi) = \{1 - \sqrt{4\phi/\pi}\}^{-1}$$

$$\lambda_c = f(\phi)\lambda_s,$$

$$\eta_{0,c} = f(\phi)\eta_{0,s} \quad (13)$$

Here, ϕ is the volume fraction of fibers, π is pi, λ_s is the neat resin time constant, η_{0s} is the neat resin zero-shear-rate viscosity, λ_c is the fiber-reinforced polymer time constant, and η_{0c} is the fiber-reinforced polymer zero-shear-rate viscosity. The modified Carreau model is then

$$\eta_c = f(\phi)\eta_{0s}[1 + (f(\phi)\lambda_s\dot{\gamma})^2]^{(n-1)/2} \quad (14)$$

The advantage of this new model is that the viscosity-shear rate relationship need only be experimentally found for the neat resin, and no additional experimentation is needed for the glass fibers. This will not only save time and expense but allow for more engineering analysis of flow geometries for composite material parts.

THE INJECTION MOLDING PROCESS

Injection molding, one of the most common operations for forming of plastic materials, has applications in the appliance, electronics, automotive, and aerospace industries. It is especially used to make automotive components from trim pieces to body panels. The injection molding process was used to mold small plaques for the Himont and DSM polypropylene materials and consists of four basic steps, shown in *Fig. 2*.

As indicated in *Fig. 2*, the plastic pellet is melted, injected into a die cavity, cooled, and the molded part is then ejected. The mechanical process involves melting, flowing, and cooling of the thermoplastic material. The melting and injecting stages take place in an injection unit, and the cooling step takes place in a hydraulic press. Thus, the injection molding machine consists of two parts: an injection unit and a hydraulic press. The injection unit can be a plunger type or a reciprocating screw. The most common of the two, the reciprocating screw with a 75 ton hydraulic press was used in our experiment. More information on injection molding can be found elsewhere (35). During our experiments a New Britain model 75-TP was used.

Experimental Equipment

The experimental set-up for the injection molding operation includes pressure transducers in the die cavity, a thermocouple at the nozzle, and data acquisition equipment. The resin was injected into a 7.55 cm by 15.1 cm by 0.3 cm cavity, via a three-step runner system, shown in *Fig. 3*.

The experimental setup for the injection molding machine involved data-acquisition equipment, including an AST 486 computer, Keithley data-acquisition cards, Dynisco pressure transducers and thermocouples, and LABTECH Notebook computer software. During the injection molding operation, the pressure traces were recorded at three locations. The first transducer is located in the nozzle of the extruder, the second is located at the middle of the cavity die, and the third transducer is at the end of the cavity. For

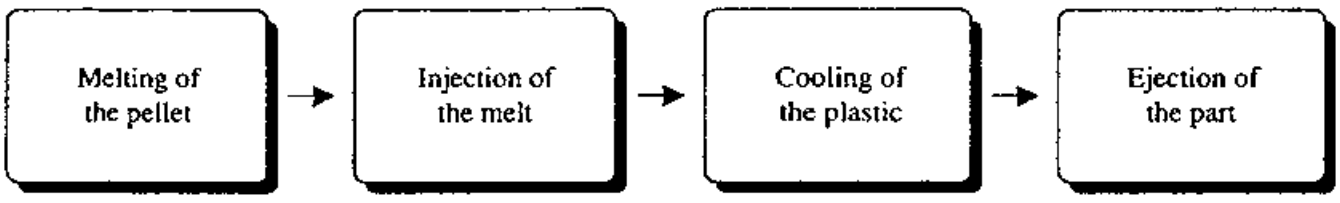

Fig. 2. Stages of the injection molding process.

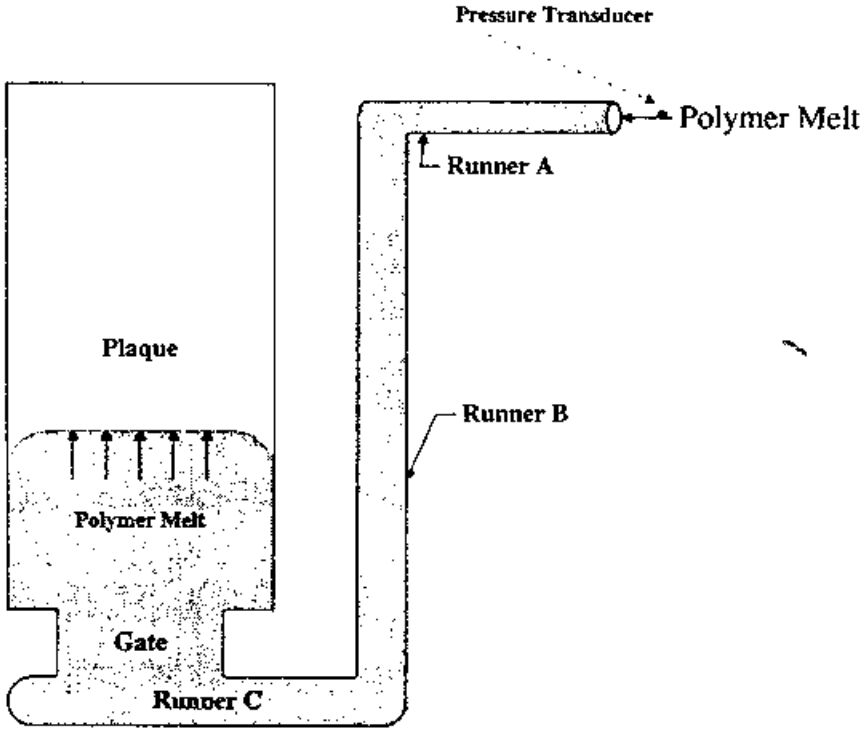

Fig. 3. Injection molding test plaque and runner geometry.

comparison purposes, the pressure trace at the nozzle is used to compare to numerical calculations. LABTECH Notebook is used to record the pressure traces, melt temperature at the nozzle, and ram location. The output data is then saved in a Lotus™ file. The experimental process is outlined below:

1. Run injection molder until steady state is reached (usually ten to fifteen parts).
2. Record the pressure, temperature, and ram-speed traces for five full shots at slow injection speed.
3. Repeat for five incomplete shots and then two air shots.
4. Repeat for fast injection speed.
5. Change material, flush, and repeat process as needed.

The full shots were used to compare filling pressure with the numerical calculations. To get a pressure at the entrance to the first runner (Runner A), the air-shot pressure first must be subtracted from the nozzle pressure. The short shots are used for measurements of the fiber orientation that will be described more fully later. The pressure traces are provided in the **Appendix** for the neat Himont resin and the neat and glass-filled DSM polypropylene materials.

Materials for Injection Molding

The materials used in the injection molding machine are two types of polypropylene, namely Himont polypropylene, and DSM polypropylene. The Himont material was available in the injection molding lab with a database of material properties, e.g., power-law viscosity coefficients. The Himont material was used as a test case for the numerical calculations of injection molding for unfilled thermoplastics. The DSM polypropylene had 0, 10, and 20 wt% short-glass fibers and was tested with a parallel-plate rheometer. The Carreau coefficients were determined from published viscosity data for the Himont material, and were determined from parallel-plate testing for the DSM material. The constants used in the numerical work are given in *Table 1*.

COMPARISON OF CALCULATED TO EXPERIMENTAL RESULTS FOR DSM POLYPROPYLENE

The rheometric work for the DSM polypropylene can be compared to the calculated viscosities using the modified Carreau model. The DSM polypropylene was provided as pellets with glass weight percentages of 0%, 10%, and 20%, with a common base resin and were injection molded into plaque form. The molded plaques were used to characterize the DSM polymer rheometrically by using a parallel-plate viscometer. The viscosity curves for the glass-filled DSM resin are shown in *Fig. 6*.

The experimental viscosities of the DSM materials were used to calculate the coefficients of the Carreau model, which were then used in the flow analysis program for the Carreau and modified Carreau model for fibers. For the neat DSM material, the comparison of the calculated Carreau model viscosity to the experimental viscosity at the reference temperature of 200°C is given in *Fig. 7*. The viscosity-shear rate relationship is well characterized by the Carreau model. The flow analysis package uses the fiber concentration function, $f(\phi)$, to describe the effects of fibers on the vis-

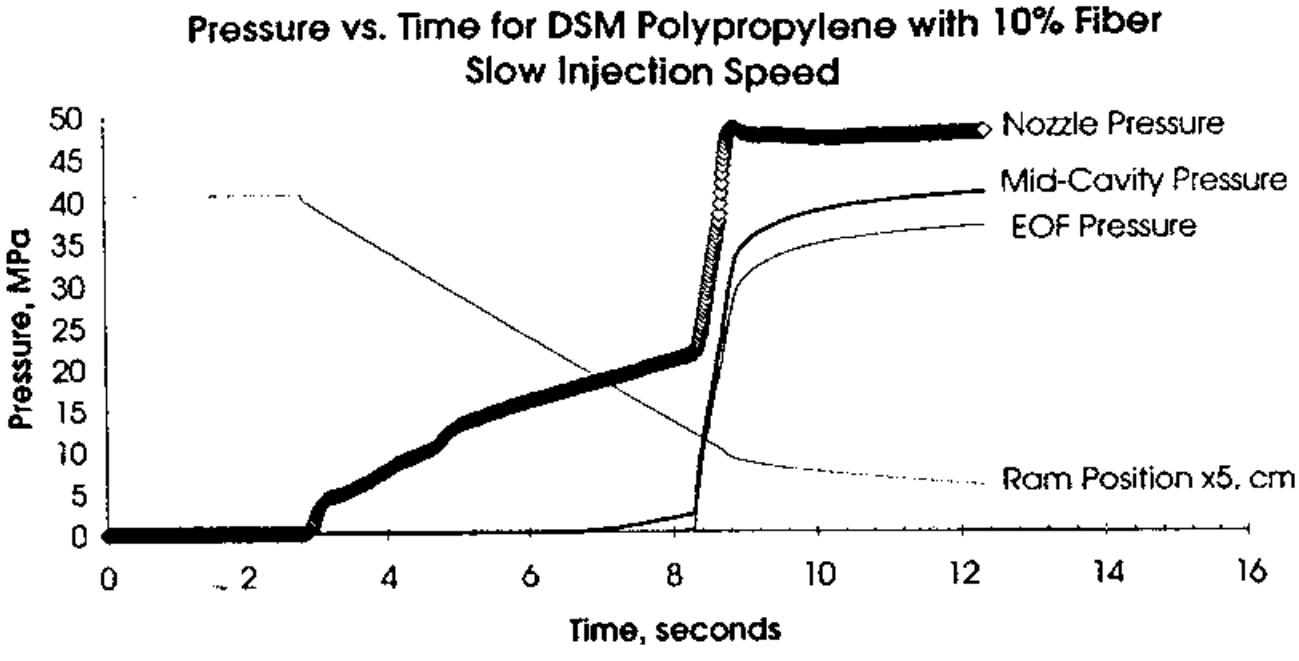

Fig. 4. Pressure transducer results for DSM polypropylene at slow injection speed. The recorded items are ram position and nozzl mid-cavity, and end-of-flow pressures.

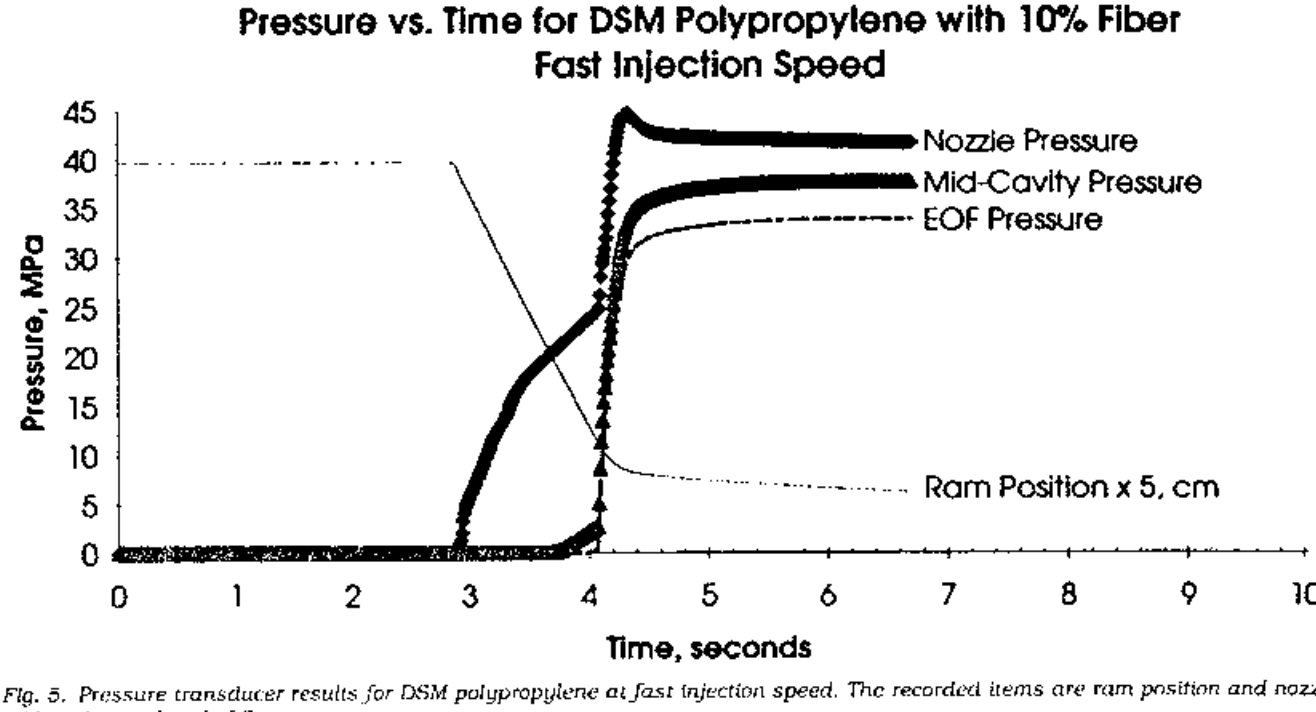

Fig. 5. Pressure transducer results for DSM polypropylene at fast injection speed. The recorded items are ram position and nozz mid-cavity, and end-of-flow pressures.

cosity. At 0% glass fibers the calculated Carreau coefficients are the same as that of the neat resin, while at higher glass concentrations, they are a product of the function $f(\phi)$ and the neat-resin coefficients. The ratio of calculated-to-actual Carreau coefficients, $f(\phi)$, λ, and η_0, are shown in *Fig. 8*.

The model over predicts the values of the Carreau coefficients for 10% fibers, as well as over predicts the viscosity ratio and under predicts the lambda ratio for 20% fibers. The true test of the model is to compa the calculated to experimental viscosity values. Tl modified Carreau model reasonably calculates the vi cosity of unfilled and glass-filled DSM polypropylen as shown in *Fig. 9*. The discrepancy between the e perimental and calculated values at high shear rate e.g., above 70 s^{-1}, can be attributed to the instabili of the glass-filled samples between the parallel plate Other higher shear-rate rheometers, such as a cap

Table 1. Constants for Temperature, Pressure, Shear Rate, and Fiber Concentration in the Modified Carreau and the Temperature and Pressure Viscosity Models.

Material	η_0, Pa-sec	λ, sec	n	b	T_b, C	β, Pa
Himont Polypropylene	1850	0.1203	0.3	9.14	227	1.5e-8
DSM Polypropylene	2900	0.17	0.33	14.37	200	1.5e-8

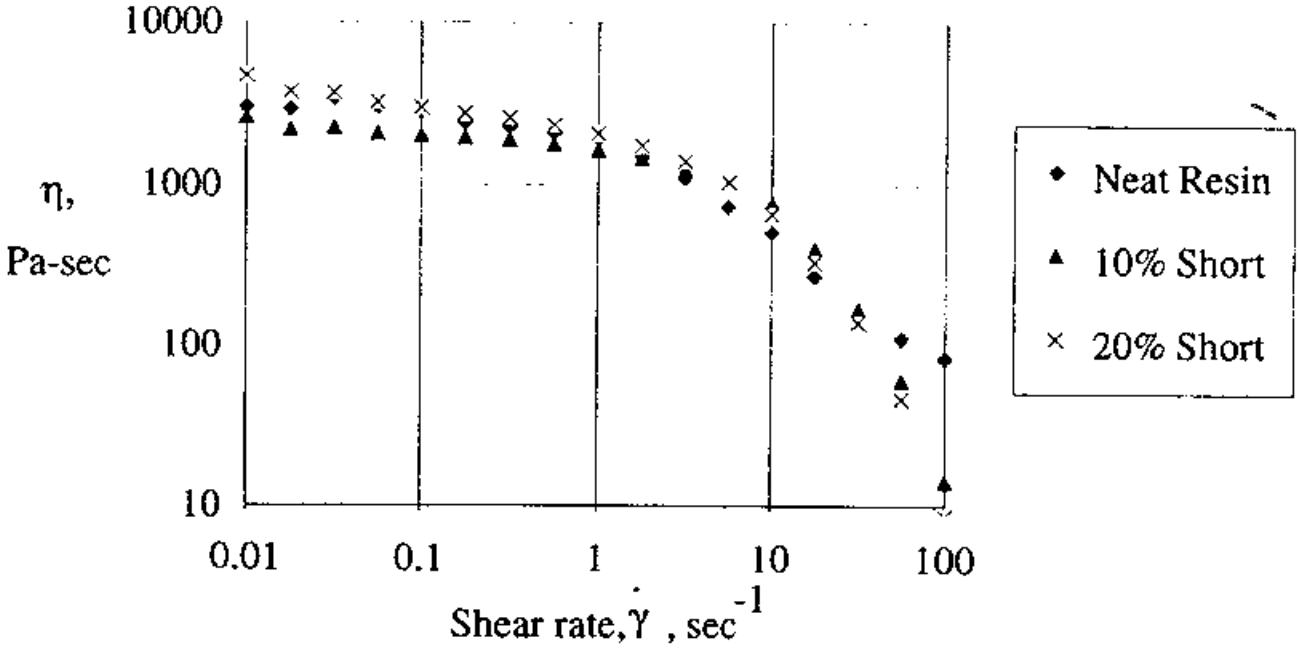

Fig. 6. DSM neat and glass-filled polypropylene viscosity vs. shear rate at 200°C.

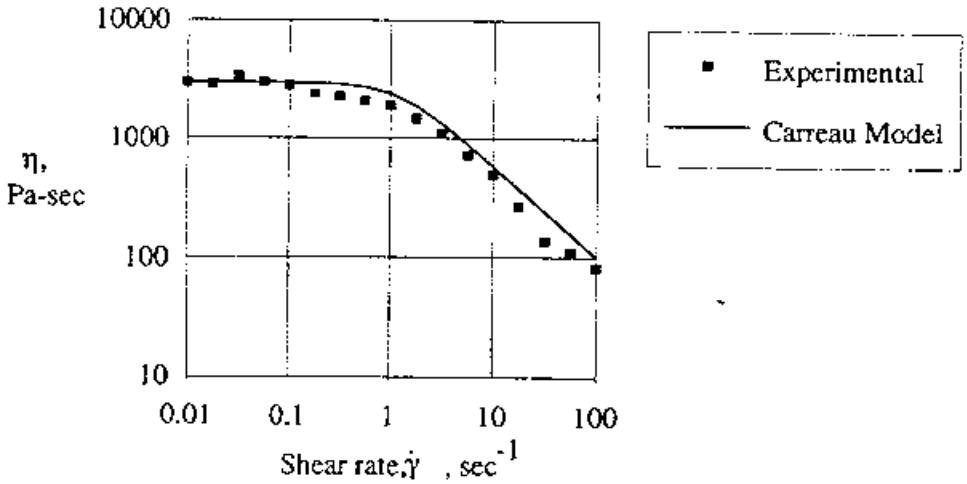

Fig. 7. DSM neat polypropylene viscosity vs. shear rate at 200°C.

lary viscometer, could reduce the error. A capillary viscometer was not readily available for our use.

NUMERICAL RESULTS AND DISCUSSION

The numerical analysis will consist of modeling the flow in a 7.75 cm by 15.25 cm plaque with a constant 0.3 cm thickness. The part geometry also includes a three-stage runner system and a gate, as given in *Fig. 3*. The pressure at the beginning of the Runner A will be compared to numerical calculations and is referred to as the fill pressure.

The modifications to the FLOW-3D programs are tested by comparing the numerical results to two cases, an experimental case with a neat resin, Himont polypropylene, and an experimental case with a glass-filled composite, DSM polypropylene.

Computing Requirements

The numerical analysis was executed on a IBM workstation, IBM *RISC 6000*. The FLOW-3D program required 35 MB of disk space. FLOW-3D has a maximum number of cells in any one direction of 200. The

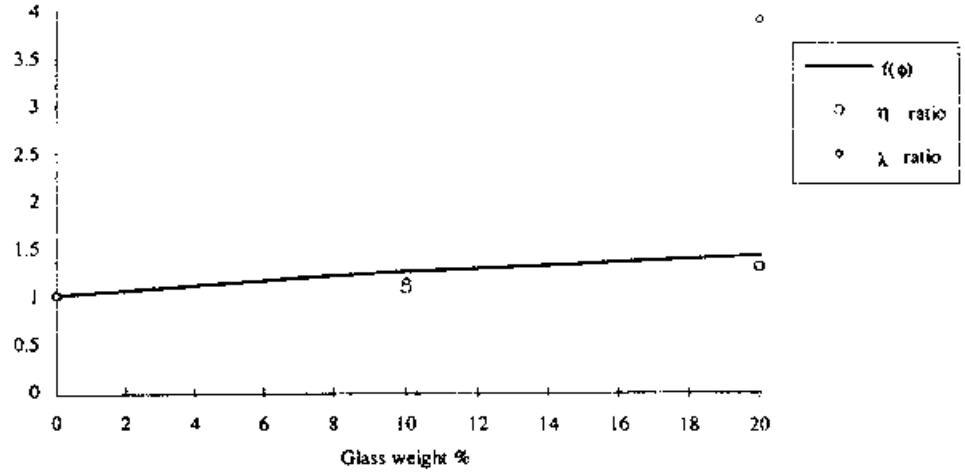

Fig. 8. DSM calculated polypropylene Carreau coefficients vs. glass %.

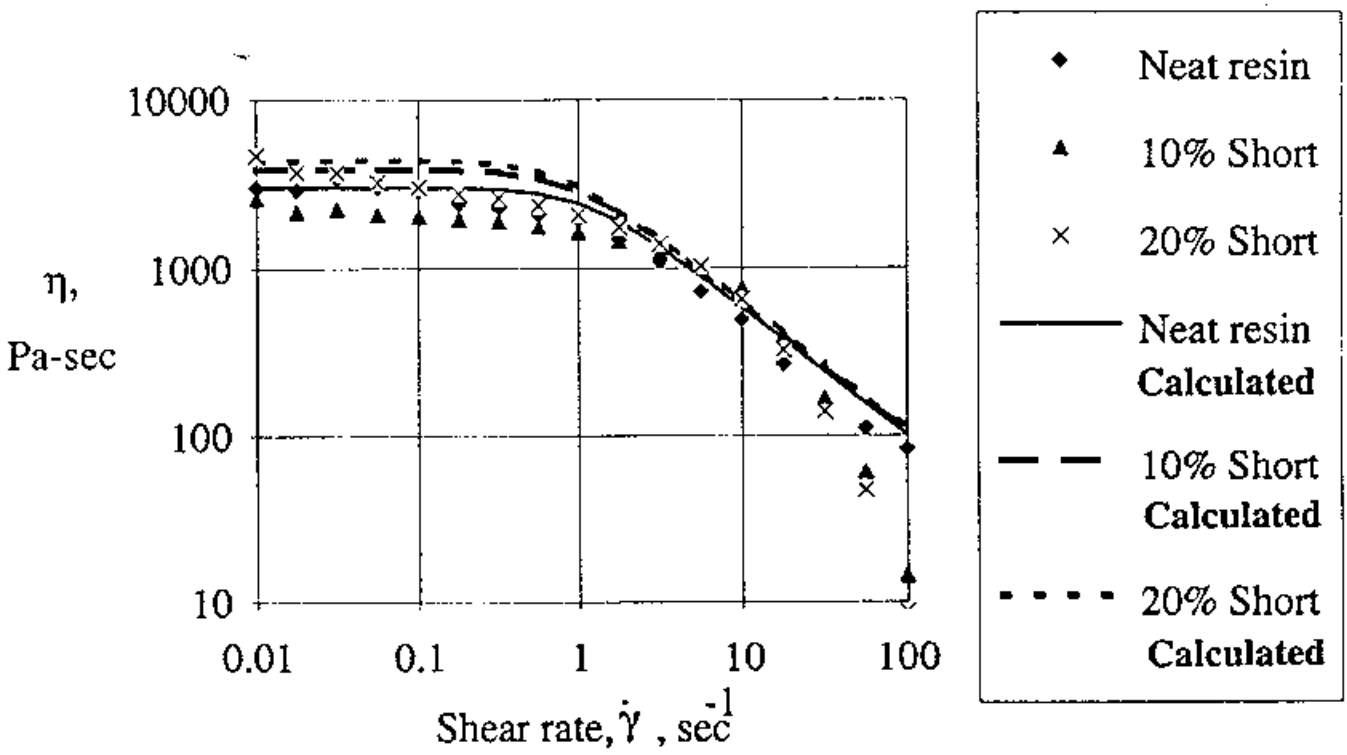

Fig. 9. DSM polypropylene experimental viscosity and modified Carreau calculated viscosity vs. shear rate.

execution time for the injection molding work (case 1 and case 2) was dependent upon the number of cells, the cell size in each direction, and the error tolerance. For case 1 and case 2, the best mesh size was with 75 cells in the flow direction, 10 cells in the half-width direction, and 1 cell in the thickness direction. The execution time was approximately 1 h, with a cumulative error of 0.5%. If the number of cells were doubled, the execution time increased three-fold with a slight reduction in cumulative error. If the number of cells were decreased by half, the error term increased to over 5%. The fill-pressures calculations for case 1 and case 2 were completed with this mesh. During the fiber-orientation calculations the mesh was 35 cells in the flow direction, 5 cells in the half-thickness direction, and 1 cell in the width direction. The fiber orientation work is essentially a 2-D slice at the centerline location along the length and through the thickness.

Case 1: Experimental Case with Neat Resin (Himont Polypropylene)

The first case compares experimental results to the FLOW-3D modified program with the pressure- and temperature-dependent viscosity model. The experimental values are averages of three injection molding pressure-drop measurements (the same for case 2). The Himont polypropylene material (melt temperature of 252°C and tool temperature of 32°C) is a standard base resin and is well characterized rheometrically in

the literature. The pressure and temperature models have been combined to the following relationship:

$$\eta(\dot{\gamma}, T, P) = \eta(\dot{\gamma})_{T=P=0} e^{-B(T-T_0)-\beta(P-P_0)} \quad (15)$$

Case 1 includes a temperature model with a dimensionless coefficient B. The coefficient B and β are experimentally determined constants. The Carreau coefficients were provided by the manufacturer. The temperature coefficient, B, was determined based upon zero-shear-rate viscosity data at several temperatures. The pressure coefficient β was found in a literature reference (36).

The results are compared to the pressure drop measurements at the beginning of runner A from the injection-molding machine for slow and fast speeds, *Figs. 10* and *11*. The *Figures* denote the pressure drop at the beginning of runner A, through the runners (A, B, and C), through the gate, and finally as the material fills the cavity. The experimental points on the *Figures* represent the pressure drop at the beginning of runner A when the flow front is at the end of the runner, at the end of the gate, and at the end of the cavity. The flow analysis is limited to a two-dimensional flow because of the thin-part molding. The analysis neglects the thickness direction and computes the flow for an axisymmetric case. The pressure drop was measured by using a transducer in the nozzle.

The comparison demonstrates good agreement between the numerical calculations and the analytical solution for slow speeds. For fast injection speeds, the FLOW-3D program over-estimates the pressure drop in the cavity. Note that the numerical work uses the temperature-pressure-dependent viscosity relationship, *Eq 15*. The purpose of the comparison was to compare numerical approximations to experiments and to identify the significance of the temperature and pressure dependency. The discrepancies between the experimental and numerical results can be attributed to the geometric simplification used to model the three runners, in which a cylindrical geometry with a constant radius was assumed for the three runners. In actuality, the first runner is a cylinder with a radius increasing with length, the second runner is a half-round with a larger radius than the first runner, and the third runner is the same as the second, though turned through a right angle. Equivalent areas were used to approximate the three runners as one runner with equivalent volume. *Figure 10* and *Figure 11* demonstrate the accuracy of the numerical calculations to be excellent at the slow speed and less accurate at the high speed. The difference in the results can be attributed in the modeling of the temperature distribution in the experiment. The program may underestimate the temperature and thus yield a higher than actual viscosity. At the faster speeds, temperature is a more significant factor that at slower speeds because of the shear-heating effects.

The importance of including the temperature dependency on the viscosity is further illustrated in *Fig. 12*. As would be expected, the faster the polymer melt is injected into the die cavity the viscosity is reduced due to shear heating, and is increased by the slight compressibility of the polymer. If the temperature effects were not included with the viscosity the numerical results would incorrectly be given by the solid curve in *Fig. 12*.

Case 2: Experimental Case with Short-Fiber-Reinforced Resin (DSM Polypropylene)

The second case compares experimental results of a DSM Polypropylene (melt temperature of 270°C and tool temperature of 32°C) to the FLOW-3D modified program with the pressure- and temperature-dependent viscosity and fiber-concentration model. The pressure and temperature models are as before. The fiber-concentration dependency is described by the modified Carreau model, and given by *Eq 14*. The Carreau coefficients were determined experimentally as previously described.

The numerical calculations are compared to actual pressure drop measurements from the injection molding machine for slow and fast speeds in *Figs. 13* and *14*. The fill pressure was measured by using a transducer at the beginning of Runner A.

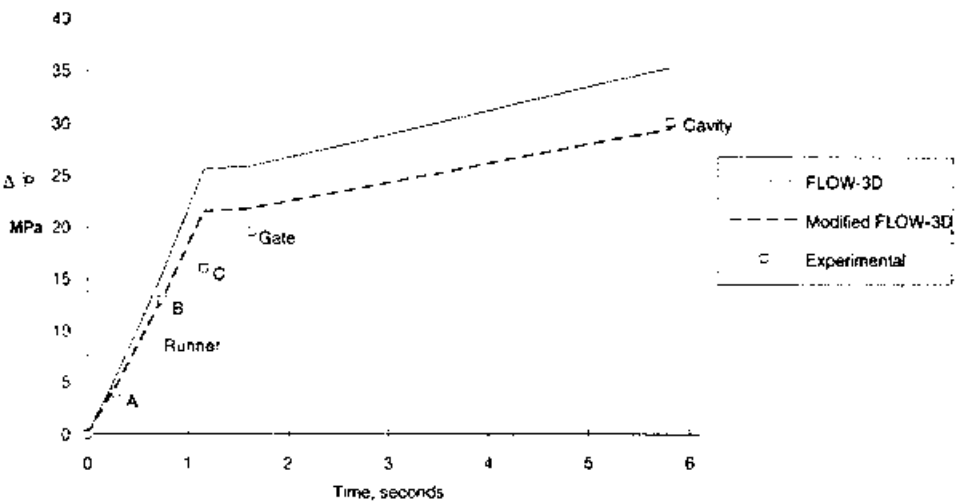

Fig. 10. Pressure drop, at the beginning of runner A, vs. injection time for Himont melt in the experimental die and runner at slow injection speed (fill time of 6 s). The open symbols represent pressure drop when the flow front reaches the stated position.

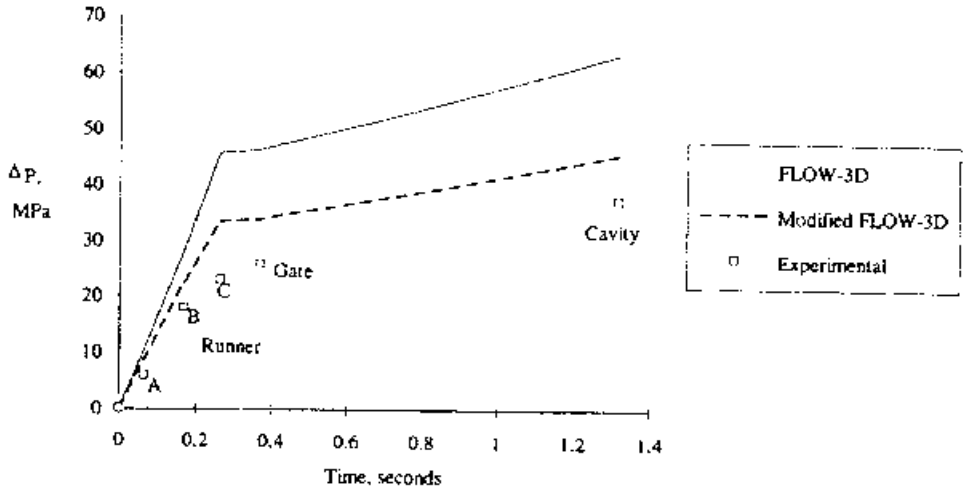

Fig. 11. Pressure drop, at the beginning of runner A, vs. injection time for Himont melt in the experimental die and runner at fast injection speed (fill time of 1.4 s). The open symbols represent pressure drop when the flow front reaches the stated position.

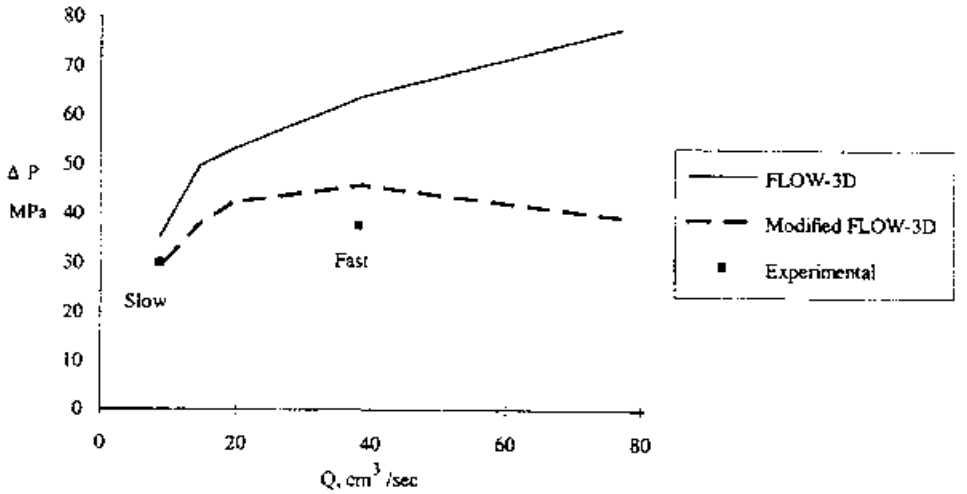

Fig. 12. Pressure drop, at the beginning of runner A, vs. flow rate for Himont melt in the experimental die and runner over a range of injection speeds.

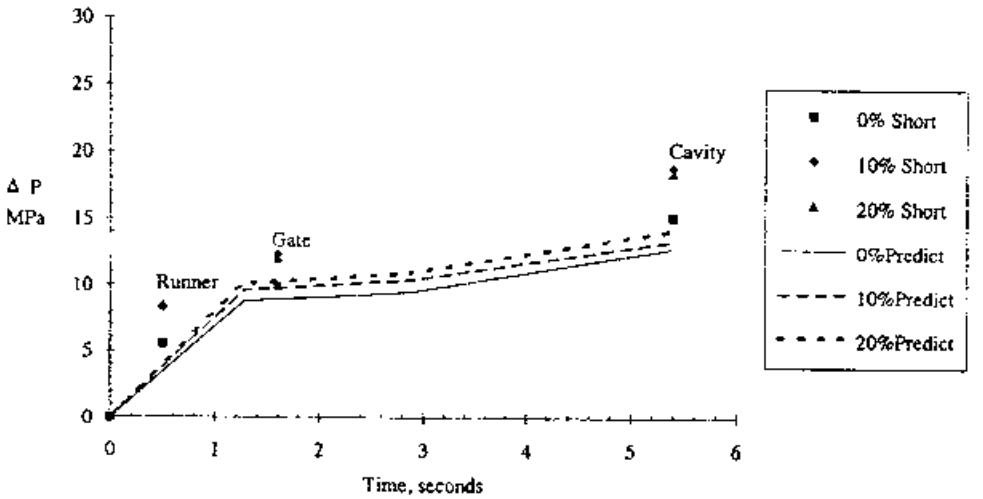

Fig. 13. Pressure drop, at the beginning of runner A, vs. time for DSM melt in the experimental die and runner at slow injection speed (fill time of 5.5 s). The darkened symbols represent pressure drop when the flow front reaches the stated position.

The comparison demonstrates reasonable agreement between the numerical calculations and the analytical solution for slow and fast speeds. For the neat resin at slow injection speed the FLOW-3D program underestimates the pressure drop, and at fast injection speed the program slightly overestimates the pressure drop. For the fiber-reinforced resin the pressure drop is captured very well for fast speed, and not very well for slow speed. Possible reasons for this discrepancy could lie in the coefficients for the heat-transfer model. The coefficient, B, was higher than in the Himont material case, and thus has larger effects

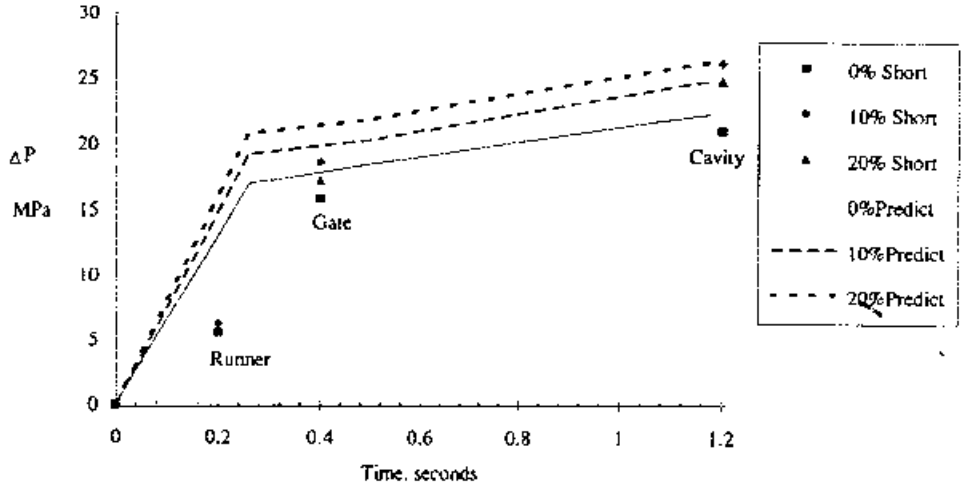

Fig. 14. Pressure drop, at the beginning of runner A, vs. time for DSM melt in the experimental die and runner at fast injection speed (fill time of 1.2 s). The darkened symbols represent pressure drop when the flow front reaches the stated position.

on the viscosity when temperature changes are significant, as at higher speeds. Note that the numerical work uses the temperature- and pressure-dependent viscosity relationship, *Eq 15*. As before, the discrepancies between the experimental and numerical results can be attributed to the geometric simplification used to model the three runners, in which a cylindrical geometry with a constant radius was assumed for the three runners. In addition, the discrepancies can be attributed to the poor viscosity fit at higher shear rates of the Carreau-Dinh/Armstrong model and the experimental data. Furthermore, viscoelastic effects can be important because of the well-known fact that elongational viscosities and normal stresses play a significant role in gate and runner geometries (37–39 and 14).

The importance of the calculation of fill pressures in an injection molding cavity for glass-filled polymers based solely upon Carreau coefficients of the neat resin and the volume fraction of fibers can be useful, and is the first to my knowledge to include fibers effects based upon a modified Carreau model. Otherwise the Carreau model coefficients must be determined from many rheometric experiments for all of the unfilled and glass-filled materials. Another interesting result is the experimental pressure drop for the 20% fibers is less than the pressure drop for the 10% fibers in both the fast speed and slow speed cases. This can be attributed to the enhanced shear thinning caused by the presence of the fibers.

CONCLUSIONS

The focus of this paper is to apply the theories and numerical techniques for injection molding of fiber-filled thermoplastics to a flow analysis computer program, and to compare the calculated results to experimental measurements. The modified computer program includes a new viscosity model with a temperature, pressure, and fiber-concentration dependency.

The overall objective of this research work is to calculate the flow front, pressure, and temperature profiles for polymer melts with and without glass fibers using a modified Carreau viscosity model. The Marker-and-Cell technique as used in FLOW-3D computer program is a useful method of calculating the free-surface flow dynamics for the filling stage of injection molding with the fountain effect. The modifications to the computer program capture the dynamics for the filling stage of glass-filled polymers and accurately calculates the flow front movement.

The comparisons between the calculated and measured pressure drop for an injection molded part are reasonable for the unfilled and glass-filled polypropylene materials. The pressure drop comparison is very good for slow fill of a base case resin, Himont polypropylene, but not as good for fast fill of the resin. The pressure drop comparison is very good for fast fill of glass-filled resin, DSM polypropylene with 10% and 20% short fibers, but not as good for slow fill of the resin and resin plus fibers. Improvements can be made by using additional temperature coefficients over a broader temperature range, incorporating viscoelasticity into the polymer model, and using viscosity coefficients at higher shear-rates. Computational time can be reduced if an implicit algorithm is developed for the heat transfer analysis. The new viscosity model for fibers is useful as an approximation for the fibers effects. The model can be improved by considering fiber-fiber interactions as described in concentrated network theories.

ACKNOWLEDGMENTS

We would like to thank Dr. Howard Cox, Dr. Martin Barone, Mr. Jim Harris, Dr. Tom Kau, Dr. Harry Kuo, Mr. Glen Novak, Mr. Dave Okonski, Dr. John Ulicny, and Dr. Mike Wzygoski of the General Motors Research Laboratory for their help and valuable discussions. Additionally, we would like to thank Mr. John Ditter and Dr. C.W. Hirt of Flow Science Inc. for their help with the FLOW-3D™ computer program.

NOMENCLATURE

a = Ratio of d_c/d.
b = Distance of the half gap thickness.
B = Temperature coefficient for a viscosity equation.
d_c = The distance between cell centers.
d = The distance between the free surface and the center of the neighbor cell.
D = Fiber diameter.
F = FLOW-3D quantity denoting the fraction of fluid within the mesh cell.
$f(\phi)$ = Dinh-Armstrong fiber-concentration function.
h = Fiber spacing in the Dinh-Armstrong expression.
i = Cell index in the x-direction.
j = Cell index in the y-direction.
k = Cell index in the z-direction.
L = Fiber length.
n = Power-law index in the Carreau expression.
p = Orientation vector.
ΔP = Pressure drop.
Q = Volumetric flow rate.
t = Time.
T = Temperature.
v = Fluid velocity vector.
∇v = Velocity gradient tensor.

Greek Symbols

γ = Shear strain.
$\dot{\gamma}$ = Shear rate.
λ = Time constant in the Carreau expression.
η = NonNewtonian viscosity.
η_r = Reduced NonNewtonian viscosity.
π = Total stress tensor ($= p\delta - \tau$).
ρ = Density.
ϕ = Volume fraction of fibers.
τ = Stress tensor.

REFERENCES

1. H. Mavridis, A. Hrymak, and J. Vlachopoulos, *Polym. Eng. Sci.*, **26,** 449 (1986).
2. G. Williams and H. Lord, *Polym. Eng. Sci.*, **15,** 569 (1986).
3. C. Huang, C. Gogos, and L. Schmidt, *Polym. Eng. Sci.*, **26,** 1457 (1986).
4. D. Harry and R. Parrott, *Polym. Eng. Sci.*, **10,** 209 (1970).
5. J. Berger and C. Gogos, *Polym. Eng. Sci.*, **13,** 102 (1972).
6. Z. Tadmor, E. Broyer, and C. Gutfinger, *Polym. Eng. Sci.*, **14,** 660 (1974).
7. C. Hieber and S. Shen, *J. Non-Newt. Fluid Mech.*, **7,** 1 (1980).
8. C. Hieber, L. Socha, S. Shen, K. Wang, and A. Isayev, *Polym. Eng. Sci.*, **23,** 20 (1983).
9. H. Chiang, C. Hieber, and K. Wang, *Polym. Eng. Sci.*, **31,** 116 (1991).
10. C. Tucker, in *Fundamentals of Computer Modeling for Polymer Processing*, Hanser Publishers, New York (1989).
11. A. Isayev, in *Injection and Compression Molding Fundamentals*, Marcel Dekker, New York (1987).
12. T. Papanastasiou, T. Scriven, and L. Macosko, *J. Non-Newt. Fluid Mech.*, **22,** 271 (1987).
13. R. Wesson, T. Papanastasiou, and J. Wilkes, *J. Rheol.*, **33,** 1047 (1989).
14. K. Loh, S. Teoh, and A. Tay, *Polym. Eng. Sci.*, **36,** 368 (1996).
15. M. Bird, S. Dinh, R. Armstrong, O. Hasagger, in *Dynamics of Polymeric Liquids*, Vol. 2, Second Edition, Wiley and Sons, New York (1987).
16. M. Doi and S. Edwards, *J. Chem. Sci. Faraday Trans.*, **74,** 1789 (1978).
17. C. Curtiss and R. Bird, *J. Chem. Phys.*, **74,** 2026 (1981).
18. P. Currie, *J. Non-Newt. Fluid Mech.*, **11,** 53 (1982).
19. FLOW-3D is a CFD flow package from Flow Science, Inc. Los Alamos, New Mexico.
20. C. Austin, in *Technical Report*, Moldflow pty., Ltd., Kilsyth, Victoria, Australia (1987).
21. C-Flow is a injection molding flow package from AC Technology Inc., Ithaca, New York.
22. T. Ghosh, M. Grmela, and P. Carreau, *Polym. Compos.*, **16,** 144 (1995).
23. S. Advani and C. Tucker, *J. Rheol.*, **31,** 751 (1987).
24. M. Gupta and K. Wang, *Polym. Eng. Sci.*, **14,** 367 (1993).
25. M. Gupta, N. Santhanam, H. Chiang, K. Himasekhar, P. Tushak, and K. Wang, In *Computer Aided Design in Composite Material Technology III*, Computational Mechanics Publications (1992).
26. R. Bay and C. Tucker, *Polymer Compos.*, **13,** 317 (1992).
27. S. Dinh and R. Armstrong, *J. Rheol.*, **28,** 207 (1984).
28. J. Greene, Ph.D. dissertation, The University of Michigan (1993).
29. J. Greene and J. Wilkes, *Polym. Eng. Sci.*, **35,** 1670 (1995).
30. J. Greene and J. Wilkes, *Polym. Eng. Sci.*, submitted (1995).
31. F. Harlow and J. Welch, *Phys. Fluids*, **8,** 2182 (1965) and F. Harlow, in *Los Alamos Scientific Laboratory Report*, LA-4289 (1969).
32. C. Hirt and J. Sicilian, *Proc. Fourth Internatl. Conf. Ship. Hydro.*, National Academy of Science, Washington, D.C. (1985).
33. Z. Tadmor and C. Gogos, in *Principles of Polymer Processing*, John Wiley and Sons, New York (1979).
34. M. Bibbo, S. Dinh, and R. Armstrong, *J. Rheol.*, **29,** 905 (1986).
35. I. Rubin, in *Injection Molding: Theory and Practice*, Wiley-Interscience, New York (1973).
36. P. Zoller, in *Encyclopedia of Polymer Science and Engineering*, Vol. 5, John Wiley and Sons, New York (1986).
37. F. Cogswell, *Polym. Eng. Sci.*, **12,** 64 (1972).
38. T. Kwon, S. Shen, and K. Wang, *Polym. Eng. Sci.*, **26,** 214 (1986).
39. C. Kwag and J. Vlachopoulos, *Polym. Eng. Sci.*, **31,** 1015 (1991).